

# Northumbria Research Link

Citation: Mei, Chao, Li, Feng, Yuan, Jinhui, Kang, Zhe, Zhang, Xianting, Wang, Kuiru, Sang, Xinzhu, Wu, Qiang, Yan, Binbin, Zhou, Xian, Wang, Liang, Yu, Chongxiu and Wai, P. K. A. (2016) High Degree Picosecond Pulse Compression in Chalcogenide-Silicon Slot Waveguide Taper. *Journal of Lightwave Technology*, 34 (16). pp. 3843-3852. ISSN 0733-8724

Published by: IEEE

URL: <http://dx.doi.org/10.1109/JLT.2016.2581823>  
<<http://dx.doi.org/10.1109/JLT.2016.2581823>>

This version was downloaded from Northumbria Research Link:  
<http://nrl.northumbria.ac.uk/27759/>

Northumbria University has developed Northumbria Research Link (NRL) to enable users to access the University's research output. Copyright © and moral rights for items on NRL are retained by the individual author(s) and/or other copyright owners. Single copies of full items can be reproduced, displayed or performed, and given to third parties in any format or medium for personal research or study, educational, or not-for-profit purposes without prior permission or charge, provided the authors, title and full bibliographic details are given, as well as a hyperlink and/or URL to the original metadata page. The content must not be changed in any way. Full items must not be sold commercially in any format or medium without formal permission of the copyright holder. The full policy is available online: <http://nrl.northumbria.ac.uk/policies.html>

This document may differ from the final, published version of the research and has been made available online in accordance with publisher policies. To read and/or cite from the published version of the research, please visit the publisher's website (a subscription may be required.)

[www.northumbria.ac.uk/nrl](http://www.northumbria.ac.uk/nrl)



# High degree picosecond pulse compression in chalcogenide-silicon slot waveguide taper

Chao Mei, Feng Li, Jinhui Yuan, Member, IEEE, Zhe Kang, Xianting Zhang, Kuiru Wang, Xinzhu Sang, Qiang Wu, Binbin Yan, Xian Zhou, Member, IEEE, Liang Wang, Chongxiu Yu, and P. K. A. Wai, Fellow, IEEE

**Abstract**—In this paper, we propose and design a chalcogenide ( $\text{As}_2\text{S}_3$ ) based slot waveguide taper with exponentially decreasing dispersion profile to realize high degree pulse compression of low power chirped solitons. Based on the waveguide taper designed, self-similar pulse compression of fundamental solitons and chirped 2-soliton breather are both investigated numerically. With self-similar pulse compression scheme, a 1 ps input pulse is compressed to 81.5 fs in 6 cm propagation. By using 2-soliton breather pulses, a 1 ps chirped pulse is compressed to 80.3 fs in just 2.54 cm. This is the first demonstration of the feasibility of high degree nonlinear pulse compression in  $\text{As}_2\text{S}_3$ -based slot waveguide taper.

**Index Terms**—Self-similar pulse compression, fundamental soliton, 2-soliton breather,  $\text{As}_2\text{S}_3$ -based slot waveguide taper.

## I. INTRODUCTION

OPTICAL pulse compression is a key technique to generate ultrashort pulses [1]-[3], which have wide applications in broadband communication systems, supercontinuum and frequency comb generation [4]-[7], ultrafast spectroscopy, and biology [8]. To compress an optical pulse in the normal dispersion regime, the pulse's spectrum should first be broadened by nonlinearity, and then de-chirped by a grating pair [9], [10]. In the anomalous dispersion regime, the evolution of high order solitons can be used to compress the pulse and expand the spectrum without a grating pair [10]-[13],

but the compression factors are limited and significant pedestal will be generated [6], [14], [15]. In comparison, adiabatic [16]-[18] and self-similar [7], [19]-[23] pulse compression can achieve high degree of compression factor with small pedestal. While adiabatic pulse compression requires a long length of fiber, self-similar compression supports high degree pulse compression in a short fiber. Recently, nonlinearity increasing photonic crystal fiber (PCF) tapers were proposed to realize the self-similar pulse compression [7], but the required peak power of the input pulse is more than kilowatt. Moreover, the fabrication of such PCF tapers is still challenging because of the difficulties in controlling the fiber profile during the drawing process.

In contrast, the technology to precisely control the geometrical size of silicon waveguides during fabrication is mature. In the last two decades, silicon photonics develops rapidly and becomes the most promising candidate for monolithic integrated optoelectronic devices [24], [25]. Specifically, the high nonlinear loss caused by two photon absorption (TPA) in silicon can be dramatically circumvented by using high contrast slot waveguides, which tightly confines the propagating light to the low index region sandwiched between silicon layers [26], [27] and low TPA materials such as chalcogenide [26]-[30]. Furthermore, because of the large intrinsic third-order nonlinearity of silicon and chalcogenide [31]-[33] and the strong field confinement, the power and propagation distance required to observe the same nonlinear phenomena as in optical fibers are significantly reduced [29], [32], [34], [35]. Besides the high nonlinearity and low TPA loss, the material dispersion of chalcogenide and silicon are also much higher than that of silica, and thus the total dispersion of the slot waveguide can be greatly tailored by varying the waveguide design and geometrical size [36]-[38].

In this paper, a chalcogenide ( $\text{As}_2\text{S}_3$ )-based slot waveguide taper with an exponentially decreasing dispersion profile is designed. The propagation dynamics of chirped soliton pulses in the taper is numerically studied by using a modified generalized nonlinear Schrödinger equation (GNLSE). Both chirped fundamental solitons and two-order solitons can be compressed in the designed waveguide taper. The paper is organized as follow. In Section II, the modified GNLSE is introduced to describe the propagation of the pulses in the  $\text{As}_2\text{S}_3$ -based slot waveguide taper. In Section III, a taper with an exponentially decreasing dispersion profile is designed. In Section IV, pulse compressions of chirped fundamental soliton

Manuscript received at March 20, 2016.

Supported by the National Natural Science Foundation of China (61307109, 61475023, and 61475131), the Beijing Youth Top-notch Talent Support Program (2015000026833ZK08), the Natural Science Foundation of Beijing (4152037), the Fund of State Key Laboratory of Information Photonics and Optical Communications (Beijing University of Posts and Telecommunications) P. R. China (IPOC2015ZC06), the Hong Kong Scholars Program 2013 (PolyU G-YZ45), and the Research Grant Council of the Hong Kong Special Administrative Region China (PolyU5263/13E).

Chao Mei and Feng Li contributed equally to this paper.

Chao Mei, Jinhui Yuan, Kuiru Wang, Xinzhu Sang, Binbin Yan, and Chongxiu Yu are with the State Key Laboratory of Information Photonics and Optical Communications (Beijing University of Posts and Telecommunications), Beijing, P. R. China (The corresponding author Jinhui Yuan, e-mail: yuanjinhui81@163.com).

Feng Li, Jinhui Yuan, Zhe Kang, Xianting Zhang, Xian Zhou, Liang Wang, and P. K. A. Wai are with the Photonics Research Centre, Department of Electronic and Information Engineering, the Hong Kong Polytechnic University, Hung Hom, Hong Kong S. A. R., P. R. China.

Feng Li, and P. K. A. Wai are also with the Hong Kong Polytechnic University Shenzhen Research Institute, Shenzhen, P. R. China.

Qiang Wu is with the Department of Physics and Electrical Engineering, Northumbria University, Newcastle upon Tyne, NE1 8ST, United Kingdom.

and two-order soliton are studied. We draw conclusions in Section V.

## II. THEORETICAL MODELS

### 1. Self-similar Compression

The propagation of an optical pulse in the  $\text{As}_2\text{S}_3$ -based slot waveguide taper can be described by a modified GNLSSE [39], [40]

$$\frac{\partial A}{\partial z} + \frac{\alpha_0}{2} A - \sum_{m \geq 2} \frac{i^{m+1} \beta_m(z)}{m!} \frac{\partial^m A}{\partial t^m} = -\frac{1}{2} \sigma_f A + i\gamma_e(z) \times \left( 1 + \frac{i}{\omega_0} \frac{\partial}{\partial t} \right) \times \left[ A(z, t) \int_0^\infty R(t') |A(z, t-t')|^2 dt' \right], \quad (1)$$

where  $A(z, t)$  is the slowly varying envelope of the electric field in a co-moving frame with group velocity  $1/\beta_1$ ,  $\alpha_0$  represents the linear loss.  $\sigma_f$  describes the free carrier effects including the free carrier absorption (FCA) and free carrier dispersion (FCD). In this paper, the duration time of the used pulses is much shorter than the free-carrier lifetime of silicon, which is about 3 ns. Such short pulse duration will only induce very small carrier-index change [37]. Besides, the peak power of the pulses used is much lower than the pump peak power needed to observe free carrier effects [41]. Thus, we neglect the effects of the FCA and FCD.  $\beta_m(z)$  is the  $m$ -th order dispersion coefficient. Self-steepening and Raman scattering are also included. The complex nonlinear coefficient  $\gamma_e = \gamma + i\alpha_2$  includes the Kerr nonlinear coefficient  $\gamma$  and the TPA loss coefficient  $\alpha_2$  of the waveguide, which should be calculated by the integrations on the whole cross-section as [2], [39], [40]

$$\gamma = \frac{\omega}{c} \iint n_2(x, y) |F(x, y)|^4 dx dy / \left( \iint |F(x, y)|^2 dx dy \right)^2, \quad (2)$$

$$\alpha_2 = \frac{1}{2} \iint \beta_{\text{TPA}}(x, y) |F(x, y)|^4 dx dy / \left( \iint |F(x, y)|^2 dx dy \right)^2,$$

where  $F(x, y)$ ,  $n_2(x, y)$ , and  $\beta_{\text{TPA}}(x, y)$  represent the distributions of the electric field, nonlinear refractive index, and TPA coefficient, respectively. The different cross-sections and mode patterns at different position  $z$  of the waveguide taper will lead to the variations of  $\gamma_e(z)$  and  $\beta_m(z)$  along the taper length.

The Raman scattering has been included in the response function

$$R(t) = (1 - f_R) \delta(t) + f_R h_R(t), \quad (3)$$

where  $f_R$  is the fractional contribution of the Raman response and assumed to be 0.1. The delayed Raman response function  $h_R(t)$  is expressed by the Green's function of a damped harmonic oscillator [42]

$$h_R(t) = \frac{\tau_1^2 + \tau_2^2}{\tau_1 \tau_2} \exp\left(-\frac{t}{\tau_2}\right) \sin\left(\frac{t}{\tau_1}\right), \quad (4)$$

where  $\tau_1$  and  $\tau_2$  correspond to the inverses of the phonon oscillation frequency and the bandwidth of the Raman gain spectrum which are 15.5 fs and 230.5 fs, respectively.

To realize self-similar pulse compression in such a waveguide taper, the taper profile should be carefully designed to control the dispersion and the nonlinearity along the taper length. In an optical waveguide governed by the parameter

varying nonlinear Schrödinger equation (NLSE)

$$i \frac{\partial A}{\partial z} - \frac{\beta_2(z)}{2} \frac{\partial^2 A}{\partial t^2} + \gamma(z) |A|^2 A = 0, \quad (5)$$

self-similar solutions [20], [21] can be found when the real nonlinear coefficient  $\gamma(z)$  is a constant and the dispersion coefficient  $\beta_2$  varies as

$$\beta_2(z) = \beta_2(0) \exp(-\sigma z), \quad (6)$$

where  $\sigma = \beta_2(0)\xi$  and  $\xi$  is the initial chirp factor of the optical pulse. The self-similar solution is written

$$A(z, t) = \left( P_0 e^{\sigma z} \right)^{1/2} \text{sech} \left[ \frac{(t-t_0) e^{\sigma z}}{T_0} \right] \exp \left[ \frac{i}{2} \xi (t-t_0)^2 e^{\sigma z} \right], \quad (7)$$

where  $P_0 = |\beta_2(0)|/(\gamma(z)T_0^2)$  is the peak power of the fundamental soliton at  $z = 0$ .  $t_0$  is the position of the pulse peak and we assume it to be zero in the following simulations. As described by Eq. (7), the pulse duration will decrease and the peak power will increase exponentially along the propagation direction in such waveguides. Most importantly, the self-similar solution keeps as the fundamental soliton at every point in propagation. The pulse compression factor, which is the ratio of the full width at half maximum (FWHM) of the pulses before and after compression, only depends on the product  $\sigma z$ . It should be pointed out that if  $\gamma(z)$  is not a constant but varies significantly along the taper length, self-similar pulse compression can still be realized by using either nonlinearity increasing [7] or a combination of dispersion and nonlinearity management schemes [20].

### 2. Chirped 2-soliton Breather Compression

Comparing with fiber tapers, accurate control of the width of waveguide taper is much easier during the fabrication process [43]. However, the length of waveguide taper is normally limited in the fabrication, which will limit the compression. Furthermore, large loss of pulse energy is unavoidable in long distance propagation because of the linear and nonlinear losses of silicon based waveguides. Thus, high degree pulse compression in a short distance is more desirable. It has been demonstrated that chirped high order solitons in a dispersion varying medium is effective in enhancing the compression in short distance [21]. Specifically, when a chirped 2-soliton breather is used, the compression factor can be enhanced by more than 3 times in a same propagation distance [21].

A chirped 2-soliton breather is a bound state of two fundamental solitons without extra binding energy. At the input ( $z = 0$ ), the pulse form is given by [21]

$$A(t) = 2 \left( P_0 \right)^{1/2} \text{sech} \left[ \frac{(t-t_0)}{T_0} \right] \exp \left[ \frac{i}{2} \xi (t-t_0)^2 \right], \quad (8)$$

where  $\xi = -4/(T_0^2\pi)$  is the chirp factor. When such a chirped 2-soliton breather is injected into a dispersion exponentially decreasing medium, the pulse will be compressed because of the combined effects of high order soliton evolution and self-similar compression. The pulse compression factor oscillates quasi-periodically along the propagation direction while the upper and lower envelopes of the oscillation increase exponentially. The lower envelope follows the compression

factor of chirped fundamental soliton in such a waveguide, e.g. the self-similar compression. We note that in contrast to fundamental chirp solitons, compression of chirped 2-soliton breathers will introduce pedestals into the pulse during compression.

### III. DESIGN OF $\text{As}_2\text{S}_3$ -BASED SLOT WAVEGUIDE TAPER

Since  $\text{As}_2\text{S}_3$  has a large nonlinear refractive index  $n_2 \sim 4.0 \times 10^{-18} \text{ m}^2/\text{W}$  [13], [31], [33] and a low TPA coefficient  $\beta_{\text{TPA}} \sim 6.2 \times 10^{-15} \text{ m/W}$  at 1550 nm [30], [44], which is three orders of magnitude lower than that of silicon [45], a slot waveguide with a thin  $\text{As}_2\text{S}_3$  layer sandwiched between two silicon layers shows multiple advantages including the low TPA loss and high nonlinearity [43]. Compared with the air gap slot waveguide which should be vertical to the surface of substrate, a solid  $\text{As}_2\text{S}_3$  layer can be parallel to the surface of substrate which is similar to traditional waveguide structure and thus easier to fabricate. Waveguide structures similar to that proposed in our paper have been reported for dispersion engineering [1]. These waveguides can be fabricated by the modified technology reported in [46] with loss as low as 0.01-0.05 dB/cm. Besides, using the thermal flow technique, the sidewall roughness and optical loss of sub-micron  $\text{As}_2\text{S}_3$  waveguides can be further reduced [47].

Fig. 1(a) shows the cross-section of the  $\text{As}_2\text{S}_3$ -based slot waveguide. The substrate is silica and other surfaces of the waveguide are surrounded by air. The  $\text{As}_2\text{S}_3$  layer has a height  $H_{\text{As}} = 20 \text{ nm}$  and the two silicon layers have a same height  $H_{\text{Si}} = 170 \text{ nm}$ . To control the dispersion coefficient, the width  $W$  of the waveguide is gradually reduced along the propagation direction of the light, as shown in Fig. 1(b).

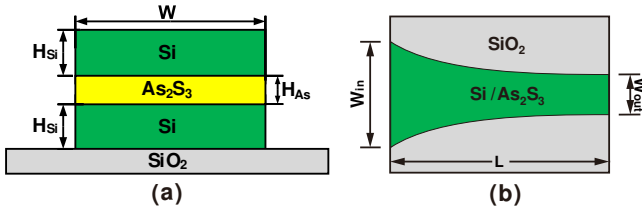


Fig. 1. (a) The typical cross-section, and (b) the top view of the designed  $\text{As}_2\text{S}_3$ -based slot waveguide taper, where  $W_{\text{in}}$  and  $W_{\text{out}}$  represent the widths of the input and output ports, respectively.

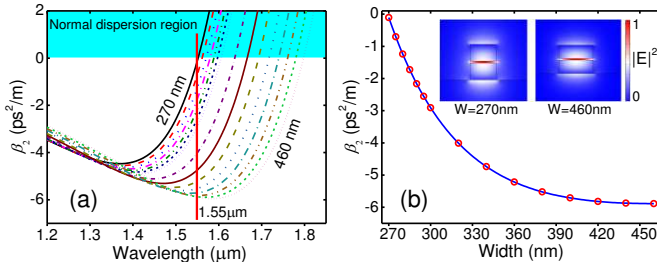


Fig. 2. (a) Dispersion curves of the fundamental mode in the designed  $\text{As}_2\text{S}_3$ -based slot waveguide with waveguide width  $W$  varying from 270 to 460 nm. The red vertical line indicates the wavelength 1550 nm. (b) The dispersion coefficient  $\beta_2$  at wavelength 1550 nm versus  $W$ . The insets show the field distributions at the input and output port of the waveguide taper.

To design a waveguide taper with exponentially decreasing dispersion that supports self-similar pulse compression, slot waveguides with different width  $W$ 's are firstly characterized

with finite element method to calculate the dispersion and nonlinear coefficients of the fundamental mode. Fig. 2(a) shows the dispersion curves  $\beta_2(\lambda)$  of the fundamental mode in the slot waveguide with different widths. From the dispersion curves  $\beta_2(\lambda)$ , higher-order dispersion coefficients can be obtained by polynomial fitting of  $\beta_2(\omega)$ . From Fig. 2(a), when the waveguide width is reduced from 460 to 270 nm, the dispersion curve is shifted towards short wavelength, and the minimum value of  $\beta_2$  increases. Because of the large slope of the dispersion curve at the long wavelength side, blue-shift of the dispersion curve leads to monotonic increasing of  $\beta_2$  at wavelength 1550 nm as indicated by the red vertical line in Fig. 2(a). Fig. 2(b) shows the variation of  $\beta_2$  at 1550 nm versus the waveguide width, where the circles are measured by finite element method and the solid curve is the spline interpolation. The dispersion coefficient  $\beta_2$  at 1550 nm varies greatly from  $-0.1087$  to  $-5.887 \text{ ps}^2/\text{m}$  when the waveguide width increases from 270 to 460 nm.

With the dispersion curve  $\beta_2(W)$  shown in Fig. 2(b), the required taper profile  $W(z)$  can be numerically calculated to satisfy the dispersion varying condition Eq. (6) for self-similar pulse compression. The red solid curve in Fig. 3(a) shows the profile  $W(z)$  which decreases from 460 to 270.9 nm along a 6 cm long taper. The corresponding exponentially decreasing dispersion  $\beta_2(z)$  varies from  $-5.887$  to  $-0.219 \text{ ps}^2/\text{m}$  as shown by the blue dashed curve in Fig. 3(a). The scaling factor  $\sigma$  is therefore  $54.86 \text{ m}^{-1}$  according to Eq. (6). From Eq. (7), such a taper will support self-similar pulse compression with a theoretical compression factor of 26.9 in ideal case.

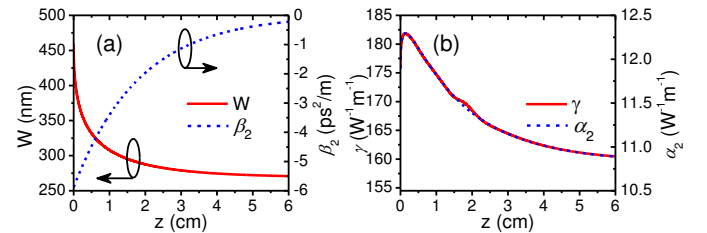


Fig. 3. (a) The waveguide width  $W$  and the corresponding dispersion  $\beta_2$  along the taper length. (b) The variations of the nonlinearity coefficient  $\gamma$  and the TPA coefficient  $\alpha_2$  along the taper length.

Besides the dispersion coefficients, the nonlinearity and TPA loss coefficient of the waveguide should also be characterized. The nonlinear refractive indices  $n_2$  of  $\text{As}_2\text{S}_3$ , silicon and silica are  $4.0 \times 10^{-18} \text{ m}^2/\text{W}$ ,  $9.0 \times 10^{-18} \text{ m}^2/\text{W}$ , and  $2.2 \times 10^{-20} \text{ m}^2/\text{W}$ , respectively. The TPA coefficient  $\beta_{\text{TPA}}$  is non-zero only in the  $\text{As}_2\text{S}_3$  and silicon regions with values  $6.2 \times 10^{-15} \text{ m/W}$  and  $5.0 \times 10^{-12} \text{ m/W}$ , respectively. In the designed waveguide taper, the variation of the electrical field distribution in different materials and the very different  $n_2$  and TPA coefficient  $\beta_{\text{TPA}}$  of Si,  $\text{As}_2\text{S}_3$  and  $\text{SiO}_2$  lead to complex variations of the nonlinear coefficient  $\gamma$  and the TPA loss  $\alpha_2$ . Fig. 3(b) shows the variations of  $\gamma$  and  $\alpha_2$  at 1550 nm along the waveguide taper which are calculated by using Eq. (2). The variations of  $\gamma$  and  $\alpha_2$  are very similar along the  $z$  direction, and they almost overlap. Compared with the monotonic change of dispersion in Fig. 3(a), the variations of  $\gamma$  and  $\alpha_2$  are not monotonic, as shown in Fig. 3(b). When  $z < 0.14 \text{ cm}$ , the values

of  $\gamma$  and  $\alpha_2$  increase from  $175.9 \text{ W}^{-1}\text{m}^{-1}$  and  $11.89 \text{ W}^{-1}\text{m}^{-1}$  to  $181.8 \text{ W}^{-1}\text{m}^{-1}$  and  $12.30 \text{ W}^{-1}\text{m}^{-1}$ , respectively. Then both of them monotonically decrease when  $z > 0.14 \text{ cm}$ . At  $z = 6 \text{ cm}$ ,  $\gamma$  and  $\alpha_2$  reach the minimum values  $160.5 \text{ W}^{-1}\text{m}^{-1}$  and  $10.89 \text{ W}^{-1}\text{m}^{-1}$ , respectively. The relative deviations of both  $\gamma$  and  $\alpha_2$  along the taper are in a range of  $\pm 6\%$ . We note that the self-similar solution in Eq. (7) is obtained under the assumptions of constant nonlinear coefficient and lossless propagation in the waveguide. Although the relative variations of the nonlinear coefficient and TPA loss coefficient along the taper length  $z$  are small, their perturbations to the self-similar propagation will also be considered.

#### IV. CHIRPED SOLITONS COMPRESSION IN $\text{As}_2\text{S}_3$ -BASED SLOT WAVEGUIDE TAPER

To study the  $\text{As}_2\text{S}_3$ -based slot waveguide taper designed in Section III, we will numerically investigate the pulse propagation in the waveguide with Eq. (1). The nonlinearity variation and TPA loss will both be considered. High order solitons, specifically 2-soliton breathers, will also be used to enhance the pulse compression.

##### 1. Self-similar Compression in a Slot Waveguide Taper

As described by the governing Eq. (5) and the analytical solution in Eq. (7), a properly chosen chirped soliton injected into the designed taper will be compressed exponentially if the nonlinearity is a constant. Since the variation of the nonlinearity in the designed taper shown in Fig. 3(b) is relatively small, the variations can be considered as a perturbation to the effective value

$$\gamma_{\text{eff}} = \frac{1}{L} \int_0^L \gamma(z) dz, \quad (9)$$

where  $\gamma(z)$  is given in Fig. 3(b). In the designed taper, the effective nonlinear coefficient  $\gamma_{\text{eff}}$  is  $167.3 \text{ W}^{-1}\text{m}^{-1}$ . If the FWHM of the pulse is 1 ps, which corresponds to  $T_0 = 567.3 \text{ fs}$ , the peak power will be  $0.1093 \text{ W}$  and the chirp factor  $\zeta = -9.32 \text{ ps}^{-2}$  to satisfy the fundamental soliton condition with  $\beta_2(0) = -5.887 \text{ ps}^2/\text{m}$ . According to Eq. (7), the theoretical compression factor in 6 cm of propagation is 26.9, and the 1 ps pulse will be compressed to 37.2 fs. We use the compression factor  $F_c$  and the compression quality factor  $Q_c$  to quantify the performance of the compression.  $F_c$  is defined as the ratio  $\text{FWHM}_{\text{in}}/\text{FWHM}_{\text{out}}$ , which is 26.9 in the ideal case. The compression quality factor  $Q_c$  is defined as  $Q_c = P_{\text{out}}/(P_{\text{in}}F_c)$  [48], where  $P_{\text{out}}$  and  $P_{\text{in}}$  are the peak powers of the output and input pulses. In the ideal case of Eq. (7), the peak power of the compressed pulse after 6 cm taper is 2.941 W. Thus, the ideal quality factor  $Q_c$  is 1.

The impacts of higher-order dispersion, nonlinear effects including self-steepening, Raman scattering and TPA loss should be considered to investigate the self-similar pulse compression in the  $\text{As}_2\text{S}_3$ -based slot waveguide taper. As discussed in Section I, the absorption loss including linear absorption and multiphoton absorption are the distinct features of silicon and chalcogenide when compared with dielectric such as silica used in most optical fibers. Here, we classify the

effects into two groups. Group I includes the up to 6-th order dispersion coefficients to model the dispersion, nonlinearity variation along the waveguide taper length, self-steepening, and Raman scattering but without any absorption loss terms. Group II is the absorption loss which includes the linear loss and TPA loss of the waveguide.

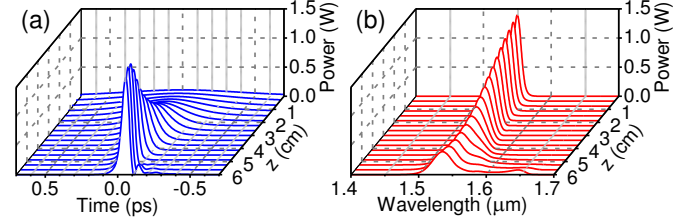


Fig. 4. Evolutions of the (a) waveform and (b) spectrum of the pulse propagating in the waveguide taper when the higher-order dispersion, higher-order nonlinearity and varying  $\gamma(z)$  are considered. The time axis of (a) is reversed to show the pulse detail.

Figure 4 shows the evolutions of the pulse waveform and spectrum in the waveguide taper modeled by Eq. (1) with  $\alpha_0 = \alpha_2 = 0$ , which includes the effects of Group I only. We observe that the pulse is compressed self-similarly for  $z < 5 \text{ cm}$ . When the pulse is compressed, both the peak power and spectral bandwidth increase. Thus the distortion induced by the higher-order effects in group I are also increased. At  $z \sim 5 \text{ cm}$ , the pulse evolution begins to gradually deviate from the self-similar compression. Although the pulse duration continues to decrease when  $z > 5 \text{ cm}$ , the rate of compression greatly slows down. At the end of the taper,  $z = 6 \text{ cm}$ , the 1-ps input pulse is compressed to 59.6 fs with  $F_c = 16.8$ . From Fig. 4(a), a satellite pulse develops rapidly near the main pulse in the temporal domain. A corresponding satellite peak is also observed in the spectra shown in Fig. 4(b). The growth of the satellite pulse is caused by the interaction of the higher-order effects in Group I. Since the satellite pulse takes away part of the energy of the main pulse, the increase of the peak power of the main pulse slowed down and even decreases when  $z > 5.5 \text{ cm}$ . The peak power of the output pulse is 1.67 W which is only 57% of that predicted in the ideal case. The corresponding compression quality  $Q_c$  is 0.91. The maximum peak power of the pulse is 1.77 W, which appears at  $z = 5.5 \text{ cm}$  with a pulse duration of 60.73 fs and a  $Q_c = 0.98$ .

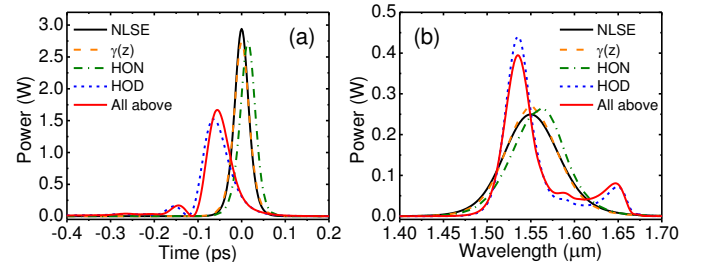


Fig. 5. Comparison of (a) the temporal waveforms and (b) the spectra of the output pulses from the waveguide taper when the varying nonlinearity  $\gamma(z)$  (orange dashed curves), higher-order dispersion (HOD, blue dashed curves) and higher-order nonlinear effects (HONs, green dash-dotted curves) including self-steepening and Raman scattering, respectively, are included. The results with only NLSE (black solid curves) and all the above effects (red solid curves) are also shown for comparison.

To characterize the impact of each effect in Group I on

self-similar compression, we investigate the pulse propagation with (i) only the varying nonlinearity, (ii) only the higher-order dispersion or (iii) only the higher-order nonlinearity including self-steepening and Raman scattering, respectively.

In Fig. 5, the temporal waveforms and spectra of the output pulses when the varying nonlinearity  $\gamma(z)$  (orange dashed curves), higher-order dispersion (HOD, blue dashed curves) and higher-order nonlinear effects (HON, green dash-dotted curves) including self-steepening and Raman scattering are compared. The results with NLSE only (black solid curves) and all of the above effects (red solid curves) are also shown for comparison.

From Fig. 5, the influence of the variation of nonlinearity is very slight. The self-steepening and Raman effects introduce a slight asymmetry on both the waveform and spectrum but without significantly changing the profiles. The spectrum is also slightly shifted towards longer wavelength by the Raman scattering. In contrast to the small deviation caused by the varying nonlinearity and the higher-order nonlinear effects, the distortions on the waveform and spectrum caused by the higher-order dispersion are significant. A small satellite pulse and a pedestal are formed by higher-order dispersion. From the dispersion curves in Fig. 2(a), the zero dispersion wavelength (ZDW) will be close to the central wavelength 1550 nm when  $W$  is close to 270 nm. Then higher-order dispersion will dominate the dispersion when the second order dispersion  $|\beta_2|$  is small.

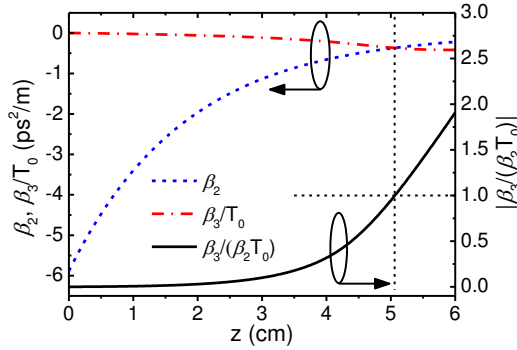


Fig. 6. Estimation and comparison of the impacts of  $\beta_2$  and  $\beta_3$  during the propagation.

To quantify the contributions of  $\beta_2$  and the HOD, where  $\beta_3$  is dominant, we plot the variations of  $\beta_2$ ,  $\beta_3/T_0$ , and  $|\beta_3/(\beta_2 T_0)|$ , which is also the ratio of the dispersion length  $L_D$  to the third order dispersion length  $L_D^{(3)}$  [2], as shown in Fig. 6. With the self-similar propagation of the pulse in the waveguide taper, the pulse duration  $T_0$  and  $|\beta_2|$  both decrease exponentially. Oppositely, the third order dispersion  $|\beta_3|$  increases along the taper. In the taper section of  $z > 5.1$  cm, the impact of  $\beta_3$  is larger than that of  $\beta_2$  as indicated by the dashed straight lines, where the spectrum of the pulse has covered the ZDW. The spectral expansion over the ZDW will trigger the generation of dispersive wave or Cherenkov radiation [49], [50]. The dispersive wave takes away part of the energy from the main pulse and hence decreases its peak power, as shown in Fig. 5(a). From Figs. 5 and 6, higher-order dispersion is the dominator to the distortion of the compressed pulse. We note that although

Group I does not include any absorption loss, they transfer energy of the main pulse to other components and decrease the power of the main pulse.

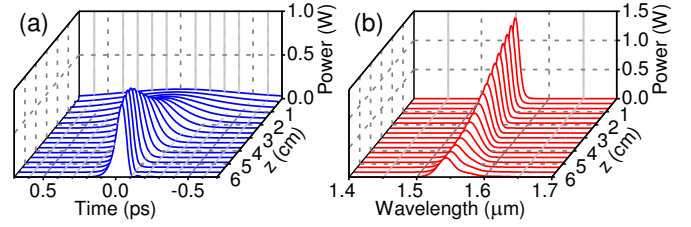


Fig. 7. The evolutions of the (a) waveform and (b) spectrum of the pulse propagating in the waveguide taper when all effects including the higher-order dispersion, higher-order nonlinearity and varying  $\gamma(z)$ , linear absorption loss and TPA loss, are all considered. The time axis of (a) is reversed to show the details of the pulse evolution.

Figure 7 shows the self-similar pulse compression when both the linear and nonlinear absorption losses are included in the simulation. The TPA loss in both the  $As_2S_3$  and  $Si$  regions has been shown in Fig. 3(b). The linear loss  $\alpha_0$  of the waveguide is assumed to 1 dB/m. The evolutions of pulse waveform and spectrum in the waveguide taper are shown in Figs. 7(a) and 7(b), respectively, where all of the effects in groups I and II are included. Compared with Fig. 4, the peak power of the output pulse is decreased further to 0.83 W, and the pulse duration is 81.5 fs. The pulse compression factor  $F_c$  is 12.3, and the quality factor  $Q_c$  is 0.62. The smaller compression factor means a narrower spectral bandwidth and hence weaker dispersive wave generation, which can be observed from the smaller satellite pulse in Fig. 7(a) and the lower side lobe on the long wavelength side in Fig. 7(b). By integration over the whole time window, about 37.8% of the input energy has been lost in the propagation which corresponds to a total loss of 2.06 dB. Since the linear loss is only 0.06 dB in the 6 cm waveguide taper, the TPA in the waveguide is the dominant loss mechanism.

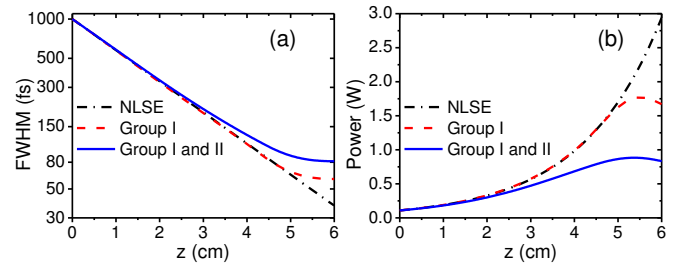


Fig. 8. The evolutions of the (a) FWHM and (b) peak power of the pulse along the propagation length in the waveguide taper with the NLSE only (black dash dotted curves), effects in Group I included (red dashed curves), or effects in Groups I and II both included (blue solid curves).

Figure 8 shows the evolutions of the FWHM and peak power of the pulse along the waveguide taper length in the ideal case (with only the NLSE), with effects in Group I, and Groups I and II both considered. In Fig. 8(a), the FWHM is plotted in logarithmic scale to show the detail near the taper output. From Fig. 8, the compression curves with only Group I effects are almost the same as those of the ideal case for  $z < 5$  cm but the differences increase rapidly when  $z > 5$  cm. When the effects in Group II are further included, as demonstrated by the blue solid

curves in Fig. 8, the absorption loss gradually deviates from the compression curve off the ideal case. As shown in Fig. 8, the absorption losses in Group II have stronger effect on the self-similar compression than the effects in Group I.

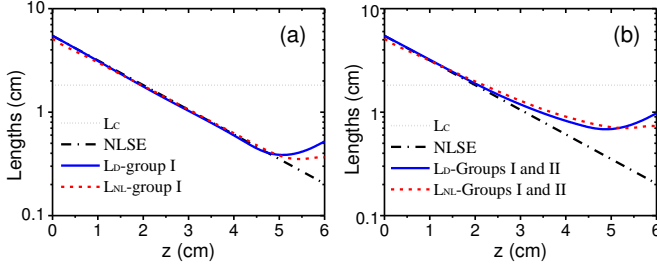


Fig. 9. The variations of the dispersion length  $L_D$  (blue solid curves) and nonlinear length  $L_{NL}$  (red dashed curves) along the propagation distance. In (a), the effects in Group I are considered. In (b), the effects in Groups I and II are considered. The black dotted lines are the chirp length  $L_C$  and the black dash dotted lines are the ideal  $L_D$  and  $L_{NL}$  when NLSE is considered only.

In ideal self-similar propagation, the fundamental soliton condition  $L_D = L_{NL}$  should be satisfied in the whole process to maintain the pulse shape, where  $L_D(z) = |T_0^2(z)/\beta_2(z)|$  and  $L_{NL}(z) = 1/[\gamma(z)P_0(z)]$  are the dispersion length and nonlinear length, respectively. Fig. 9 plots the  $L_D$  and  $L_{NL}$  versus  $z$  calculated from the pulse duration and peak power shown in Fig. 8. The ideal chirp length  $L_C = 1/\sigma$  is also plotted to estimate the contributions of nonlinearity and dispersion in the self-similar compression [51]. Fig. 9(a) shows that  $L_D$  and  $L_{NL}$  are very close to those in ideal case for  $z < 5$  cm if only the effects in group I are included. When losses are included as shown in Fig. 9(b), although  $L_D$  and  $L_{NL}$  deviate from the ideal case gradually, but both of the deviations are on the same side of the ideal curve and  $L_D$  is close to  $L_{NL}$  in propagation.

In summary, an input pulse with duration 1 ps can be compressed to 81.5 fs with a  $Q_c = 0.62$  in the proposed waveguide taper. In most part of the propagation, the pulse is compressed self-similarly. The linear and TPA losses of the waveguide have decreased the pulse energy by  $\sim 2.06$  dB which is the dominant perturbation to the self-similar compression. If the effects of loss are neglected, the pulse can be compressed to 60.73 fs with a  $Q_c = 0.98$  in 5.5 cm of taper. Hence, the deviation caused by the TPA loss should be carefully considered in further design of such waveguide taper for self-similar compression. Higher-order dispersion is another dominant perturbation to the self-similar compression. When  $|\beta_3/(\beta_2 T_0)|$  becomes to larger than 1 with the simultaneous decreasing of  $|\beta_2|$  and  $T_0$ , the contribution of higher-order dispersion becomes important and finally destroys the self-similar propagation by generating remarkable dispersive wave. Thus, unless the higher-order dispersion can be reduced by using flat-dispersion waveguides [37],  $|\beta_2|$  should not be excessively reduced in self-similar pulse compression.

## 2. Chirped 2-Soliton Breather Compression in a Slot Waveguide Taper

From the previous section, the TPA loss of the waveguide is the dominant effect that affects the self-similar propagation. Short propagation distance in the taper is preferred to avoid the

high energy loss. Furthermore, a 6 cm long waveguide taper is still difficult to fabricate. Even without taking loss into account, the dispersion  $|\beta_2|$  should not be reduced too much to avoid the generation of dispersive wave, which also suggests a shorter propagation distance in the designed taper. Thus, a high degree pulse compression in a short distance of the waveguide taper is desirable. It has been shown that the compression factor of self-similar compression for the same waveguide length can be enhanced by more than 3 times if 2-soliton breather is used [21]. For 2-soliton breathers, the periodic higher-order soliton evolution accompanies the self-similar compression. To utilize 2-soliton breathers to enhance pulse compression in the same waveguide taper, the peak power of the input 1 ps pulse is chosen as 0.4372 W, which is 4 times of that used in Section 4.1 in accordance to Eq. (7). The chirp factor  $\zeta = -3.96$  ps<sup>-2</sup>.

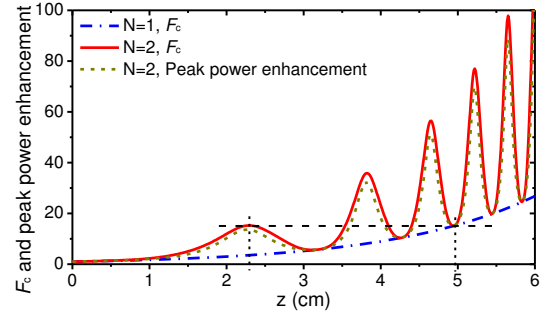


Fig. 10. The evolutions of  $F_c$  for a fundamental soliton (blue dash-dotted curve) and 2-soliton breather (red solid curve), and peak power enhancement factor of the 2-soliton breather (green dashed curves) versus waveguide taper length modeled with the ideal NLSE.

Figure 10 shows the evolution of  $F_c$  for 1-soliton (blue dash-dotted curves) and 2-soliton breather (red solid curves), and the evolution of peak power enhancement factor of 2-soliton breather (green dashed curves), which are modeled with the ideal NLSE in Eq. (5). The mismatch between the  $F_c$  and peak power enhancement curves implies the deviation of the pulse shape from the hyperbolic secant profile. The  $F_c$  curve of the 2-soliton breather oscillates along the propagation direction with minima located on the  $F_c$  curve of the fundamental soliton. From Fig. 10, a compression factor  $F_c = 15.2$  can be reached at  $z \approx 2.3$  cm by using chirped 2-soliton breather or  $z \approx 5$  cm by using chirped 1-soliton. The maximum and minimum points of  $F_c$  in Fig. 10 can be approximately predicted by calculating the higher-order soliton period [2] and assuming exponentially decreasing  $T(z)$  and  $|\beta_2(z)|$  as

$$L_k = \frac{1}{\sigma} \ln \left[ 1 + \frac{k\sigma T_0^2(0)\pi}{4|\beta_2(0)|} \right], \quad (10)$$

where  $k = 1, 3, 5, \dots$  represents the maximum points and  $k = 2, 4, 6, \dots$  represents the minimum points. The predicted extrema for the first two periods are 2.21, 3.18, 3.81 and 4.27 cm, respectively, which agree well with the curve shown in Fig. 10.

Fig. 11 shows the evolutions of the waveform and spectrum of the 2-soliton breather pulse where all other parameters and the effects included are the same as those used in Fig. 7. From Fig. 11(a), the input 1 ps pulse is compressed in the waveguide taper quickly. The pulse width reaches the minimum 80.3 fs at  $z = 2.54$  cm. The corresponding output peak power is 2.95 W.

Different from the quasi-monotonic decreasing of pulse width with the fundamental soliton shown in Fig. 7, the pulse width of the 2-soliton breather oscillates along the propagation direction. The maximum peak power of 3.08 W is observed at  $z = 2.4$  cm which is slightly before than the point of narrowest pulse width. The difference of the evolutions of 2-soliton breather and fundamental soliton is more pronounced in the spectrum as shown in Fig. 11(b). The spectrum splits, and then recovers with a small pedestal generated during the propagation, which is more complex than that of the fundamental soliton shown in Fig. 7(b). At  $z = 2.54$  cm where the narrowest pulse duration is observed, the spectrum has two high side lobes and a low peak at the center wavelength.

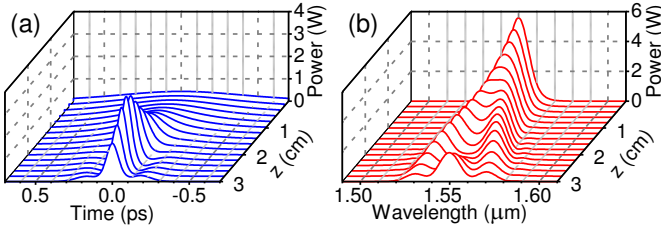


Fig. 11. Evolutions of the (a) waveform and (b) spectrum of the 2-soliton breather pulse in the waveguide taper including the effects of varying nonlinear coefficient, higher-order dispersions, higher-order nonlinear effects, TPA and linear losses of the waveguide.

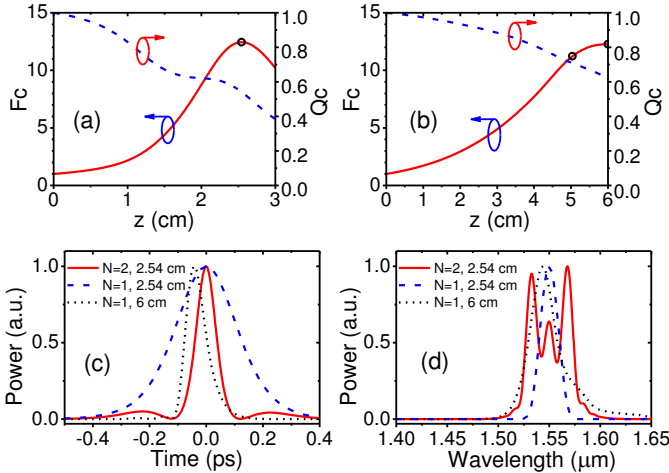


Fig. 12. The variations of compression factor  $F_c$  (red solid curves) and compression quality factor  $Q_c$  (blue dashed curves) along propagations with (a) 2-soliton breather and (b) fundamental soliton. (c) and (d) show the temporal waveforms and spectra of the pulses at  $z = 2.54$  cm with a 2-soliton breather (red solid curves), and at  $z = 2.54$  cm (blue dashed curves) and 6 cm (black short dashed curves) with a fundamental soliton, respectively.  $N$  is the soliton order. The intensities of the curves in (c) and (d) have been normalized for comparison.

Besides, Fig. 12(a) plots the variations of the compression factor  $F_c$  (red solid curves) and the quality factor  $Q_c$  (blue dashed curves) of the 2-soliton breather. Corresponding variations of the fundamental soliton are shown in Fig. 12(b) for comparison. Using the 2-soliton breather, we obtain a compression factor  $F_c = 12.45$  in just 2.54 cm, which is lower than the ideal case given in Fig. 10 and larger than the  $F_c$  value 12.3 obtained with the fundamental soliton in 6 cm long of waveguide taper. The corresponding  $Q_c = 0.541$  is slightly lower than the value 0.62 obtained with the fundamental soliton. The energy loss in the 2-soliton breather compression is 2.13

dB which is similar to that of the fundamental soliton compression.

Figs. 12(c) and 12(d) plot the waveforms and spectra, respectively, of the compressed pulse at  $z = 2.54$  cm with the 2-soliton breather and at  $z = 2.54$  and 6 cm with the fundamental soliton. The intensities of the curves in Figs. 12(c) and 12(d) have been normalized for better comparison. The output waveform with 2-soliton breather has symmetric pedestal on both sides of the main pulse which is similar to that of 2-soliton breather evolution in uniform waveguides. The output pulse at  $z = 6$  cm with the fundamental soliton has comparable pulse duration but without significant pedestal. The pulse at  $z = 2.54$  cm with the fundamental soliton has a much larger pulse duration of  $\sim 257$  fs. Thus, adoption of the 2-soliton breather compression has enhanced the compression factor by 3.2 times with the same propagation length. In Fig. 12(c), the pulse with  $N = 1$  and  $z = 6$  cm is asymmetric and retarded by several tens of femtoseconds but the peak of the pulse with  $N = 2$  remains at  $t = 0$ . The pulse retardation indicates a shift of the central wavelength, as shown in Fig. 12(d).

In this section, we demonstrated that with a properly designed waveguide taper, a chirped picosecond input pulse is nonlinearly compressed by a factor of  $\sim 12.45$ . We note that such high degree nonlinear compression will be affected by deviations of the input pulse parameters from the ideal values in realization. Although the initial chirp of the input pulse is important in the self-similar pulse compression, it was demonstrated that the self-similar pulse compression will not be significantly affected if deviation of the initial chirp is within  $\sim \pm 20\%$  [51]. It has also been shown that the pulse compression is quite tolerant to deviation of the pulse shape from hyperbolic secant profile. Even an input Gaussian pulse will not significantly change the pulse compression [52]. However, the pulse compression is rather sensitive to the peak power of the input pulse [51]. Thus in experiments, a variable optical attenuator should be used to adjust the pulse power to optimize the pulse compression.

## V. CONCLUSION

In conclusion, we proposed and designed an  $As_2S_3$ -based slot waveguide taper with exponentially decreasing dispersion profile to realize high degree pulse compression of chirped solitons. The dispersion, nonlinearity, and TPA of the waveguide with different widths are characterized by using the finite element method. Based on the waveguide taper designed, self-similar pulse compression of chirped fundamental soliton and 2-soliton breather are modeled with GNLSE. With self-similar pulse compression, a 1 ps input pulse can be compressed by a factor of 12.3 to 81.5 fs after propagation in just 6 cm of waveguide taper. In the compression, the TPA loss of the waveguide and the generation of dispersive wave dominated by higher-order dispersion are the major perturbations to the self-similar propagation. To avoid the generation of dispersive wave,  $\beta_3/(\beta_2 T_0) \ll 1$  should be guaranteed during the propagation. By adopting 2-soliton breather pulse compression, a 1 ps chirped pulse can be



compressed by a factor of 12.45 to 80.3 fs after propagation in just 2.54 cm of the waveguide taper. The high degree pulse compression in the designed waveguide taper will enable us to adopt low power picosecond laser pulses as the sources of photonic chip to investigate the ultrafast nonlinear optical phenomena and all-optical signal processing.

## REFERENCES

- [1] F. X. Kärtner, "Chapter 3 few-cycle pulse by external compression," in *Few-cycle laser pulse generation and its applications*. Berlin, Germany: Springer, 2004, pp. 138-171.
- [2] G. P. Agrawal, "Chapter 5 optical soliton," in *Nonlinear fiber optics*. Fifth ed. San Francisco, CA, USA: Academic, 2013, pp. 88-101.
- [3] M. E. Fermann and I. Hartl, "Ultrafast fibre lasers," *Nat. Photon.*, vol. 7, pp. 868-874, Oct. 2013.
- [4] J. W. Nicholson, A. D. Yablon, M. F. Yan, P. Wisk, R. Bise, D. J. Trevor, J. Alonzo, T. Stockert, J. Fleming, E. Monberg, F. Dimarcello, and J. Fini, "Coherence of supercontinua generated by ultrashort pulses compressed in optical fibers," *Opt. Lett.*, vol. 33, no. 18, pp. 2038-2040, Sept. 2008.
- [5] J. M. Dudley and J. R. Taylor, "Chapter 6 Supercontinuum generation and nonlinearity in soft glass fibers," in *Supercontinuum generation in optical fibers*. Cambridge, UK: Cambridge University, 2010, pp. 82-119.
- [6] Q. Li, J. N. Kutz, and P. K. A. Wai, "High-degree pulse compression and high-coherence supercontinuum generation in a convex dispersion profile," *Opt. Commun.*, vol. 301-302, pp. 29-33, Apr. 2013.
- [7] F. Li, Q. Li, J. Yuan, and P. K. A. Wai, "Highly coherent supercontinuum generation with picosecond pulses by using self-similar compression," *Opt. Express.*, vol. 22, no. 22, pp. 27339-27354, Oct. 2014.
- [8] J. Rehbinder, L. Brückner, A. Wipfler, T. Buckup, and M. Motzkus, "Multimodal nonlinear optical microscopy with shaped 10 fs pulses," *Opt. Express.*, vol. 22, no. 23, pp. 28790-28797, Nov. 2014.
- [9] T. Südmeyer, F. Brunner, E. Innerhofer, R. Paschotta, K. Furusawa, J. C. Baggett, T. M. Monro, D. J. Richardson, and U. Keller, "Nonlinear femtosecond pulse compression at high average power levels by use of a large-mode-area holey fiber," *Opt. Lett.*, vol. 28, no. 20, pp. 1951-1953, Oct. 2003.
- [10] K. F. Mak, J. C. Travers, N. Y. Joly, A. Abdolvand, and P. St. J. Russell, "Two techniques for temporal pulse compression in gas-filled hollow-core kagomé photonic crystal fiber," *Opt. Lett.*, vol. 38, no. 18, pp. 3592-3595, Sept. 2013.
- [11] K. C. Chan, "Short pulse generation by higher order soliton-effect compression: effects of optical fiber characteristics," *IEEE J. Quantum Electron.*, vol. 31, no. 12, pp. 2226-2235, Dec. 1995.
- [12] A. A. Amorim, M. V. Tognetti, P. Oliveira, J. L. Silva, L. M. Bernardo, F. X. Kärtner, and H. M. Crespo, "Sub-two-cycle pulses by soliton self-compression in highly nonlinear photonic crystal fibers," *Opt. Lett.*, vol. 34, no. 24, pp. 3851-3853, Dec. 2009.
- [13] A. Ben Salem, R. Cherif, and M. Zghal, "Soliton-self compression in highly nonlinear chalcogenide photonic nanowires with ultralow pulse energy," *Opt. Express.*, vol. 19, no. 21, pp. 19955-19966, Sept. 2011.
- [14] F. K. Fatemi, "Analysis of nonadiabatically compressed pulses from dispersion-decreasing fiber," *Opt. Lett.*, vol. 27, no. 18, pp. 1637-1639, Sept. 2002.
- [15] Q. Li, J. N. Kutz, and P. K. A. Wai, "Cascaded higher-order soliton for non-adiabatic pulse compression," *J. Opt. Soc. Am. B.*, vol. 27, no. 11, pp. 2180-2189, Nov. 2010.
- [16] M. D. Pelusi and H. F. Liu, "Higher order soliton pulse compression in dispersion-decreasing optical fibers," *IEEE J. Quantum Electron.*, vol. 33, no. 8, pp. 1430-1438, Aug. 1997.
- [17] M. L. V. Tse, P. Horak, J. H. V. Price, F. Poletti, F. He, and D. J. Richardson, "Pulse compression at 1.06 microm in dispersion-decreasing holey fibers," *Opt. Lett.*, vol. 31, no. 23, pp. 3504-3506, Dec. 2006.
- [18] J. C. Travers, J. M. Stone, A. B. Rulkov, B. A. Cumberland, A. K. George, S. V. Popov, J. C. Knight, and J. R. Taylor, "Optical pulse compression in dispersion decreasing photonic crystal fiber," *Opt. Express.*, vol. 15, no. 20, pp. 13203-13211, Sept. 2007.
- [19] V. I. Kruglov, A. C. Peacock, and J. D. Harvey, "Exact self-similar solutions of the generalized nonlinear Schrödinger equation with distributed coefficients," *Phys. Rev. Lett.*, vol. 90, no. 11, pp. 113902-2-113902-4, Mar. 2003.
- [20] V. I. Kruglov, A. C. Peacock, and J. D. Harvey, "Exact solutions of the generalized nonlinear Schrödinger equation with distributed coefficients," *Phys. Rev. E.*, vol. 71, pp. 056619-1-056619-10, May. 2005.
- [21] K. Senthilnathan, K. Nakkeeran, Q. Li, and P. K. A. Wai, "Pedestal free pulse compression of chirped optical solitons," *Opt. Commun.*, vol. 285, pp. 1449-1455, Nov. 2012.
- [22] S.-H. Im, D. Méchin, V. I. Kruglov, and J. D. Harvey, "Experimental demonstration of self-similar pulse compression and amplification," in *Nonlinear Guided Waves and Their Applications*, 2005, WC6.
- [23] D. Méchin, S.-H. Im, V. I. Kruglov, and J. D. Harvey, "Experimental demonstration of similariton pulse compression in a comblike dispersion-decreasing fiber amplifier," *Opt. Lett.*, vol. 31, no. 14, pp. 2106-2108, Jul. 2006.
- [24] R. Soref, "The past, present, and future of silicon photonics," *IEEE J. Sel. Top. Quantum Electron.*, vol. 12, no. 6, pp. 1678-1687, Nov. 2006.
- [25] B. Jalali and S. Fathpour, "Silicon Photonics," *J. Lightwave Technol.*, vol. 24, no. 12, pp. 4600-4615, Dec. 2006.
- [26] Q. Xu, V. R. Almeida, R. R. Panepucci, and M. Lipson, "Experimental demonstration of guiding and confining light in nanometer-size low-refractive-index material," *Opt. Lett.*, vol. 29, no. 14, pp. 1626-1628, Jul. 2004.
- [27] V. R. Almeida, Q. Xu, C. A. Barrios, and M. Lipson, "Guiding and confining light in void nanostructure," *Opt. Lett.*, vol. 29, no. 11, pp. 1209-1211, Jun. 2004.
- [28] L. Zhang, Y. Yue, Y. Xiao-Li, J. Wang, R. G. Beausoleil, and A. E. Willner, "Flat and low dispersion in highly nonlinear slot waveguides," *Opt. Express.*, vol. 18, no. 12, pp. 13187-13193, Jun. 2010.
- [29] J. Leuthold, W. Freude, J.-M. Brosi, R. Baets, P. Dumon, I. Biaggio, M. L. Scimeca, F. Diederich, B. Frank, and C. Koos, "Silicon organic hybrid technology - a platform for practical nonlinear optics," *Proceedings of the IEEE*, vol. 97, no. 7, pp. 1304-1316, Jul. 2009.
- [30] W. Zhang, S. Serna, N. Dubreuil, and E. Cassan, "Nonlinear optimization of slot Si waveguides: TPA minimization with FOM<sub>TPA</sub> up to 4.25," *Opt. Lett.*, vol. 40, no. 7, pp. 1212-1215, Apr. 2015.
- [31] J. M. Harbold, F. O. Ilday, F. W. Wise, J. S. Sanghera, V. Q. Nguyen, L. B. Shaw, and I. D. Aggarwal, "Highly nonlinear As-S-Se glasses for all-optical switching," *Opt. Lett.*, vol. 27, no. 2, pp. 119-121, Jan. 2002.
- [32] M. D. Pelusi, V. G. Ta'eed, M. R. E. Lamont, S. Madden, D.-Y. Choi, B. Luther-Davies, and B. J. Eggleton, "Ultra-high nonlinear As<sub>2</sub>S<sub>3</sub> planar waveguide for 160-Gb/s optical time-division demultiplexing by four-wave mixing," *IEEE Photon. Technol. Lett.*, vol. 19, no. 19, pp. 1496-1498, Oct. 2007.
- [33] M. Asobe, T. Kanamori, and K. Kubodera, "Applications of highly nonlinear chalcogenide glass fibers in ultrafast all-optical switches," *IEEE J. Quantum Electron.*, vol. 29, no. 8, pp. 2325-2333, Aug. 1993.
- [34] Q. Lin, O. J. Painter, and G. P. Agrawal, "Nonlinear optical phenomena in silicon waveguides: modeling and applications," *Opt. Express.*, vol. 15, no. 25, pp. 16604-16644, Nov. 2007.
- [35] P. Muellner, M. Wellenzohn, and R. Hainberger, "Nonlinearity of optimized silicon photonic slot waveguides," *Opt. Express.*, vol. 17, no. 11, pp. 9282-9287, May. 2009.
- [36] S. Mas, J. Caraquitena, J. V. Galán, P. Sanchis, and J. Martí, "Tailoring the dispersion behavior of silicon nanophotonic slot waveguides," *Opt. Express.*, vol. 18, no. 20, pp. 20839-20844, Oct. 2010.
- [37] L. Zhang, Y. Yue, R. G. Beausoleil, and A. E. Willner, "Flattened dispersion in silicon slot waveguides," *Opt. Express.*, vol. 18, no. 12, pp. 20529-20534, Jun. 2010.
- [38] D. Castelló-Lurbe, V. Torres-Company, and E. Silvestre, "Inverse dispersion engineering in silicon waveguides," *J. Opt. Soc. Am. B.*, vol. 31, no. 8, pp. 1829-1835, Aug. 2014.
- [39] L. Yin, Q. Lin, and G. P. Agrawal, "Soliton fission and supercontinuum generation in silicon waveguides," *Opt. Lett.*, vol. 32, no. 4, pp. 391-393, Feb. 2007.
- [40] Y. Zhang, H. Liu, Q. Sun, N. Huang, and Z. Wang, "Supercontinuum generation in strip/slot hybrid waveguide with flat and low dispersion," *Appl. Opt.*, vol. 54, no. 15, pp. 4850-4856, May. 2015.
- [41] L. Zhang, Q. Lin, Y. Yue, Y. Yan, R. G. Beausoleil and A. E. Willner, "Silicon waveguide with four zero-dispersion wavelengths and its

- application in on-chip octave-spanning supercontinuum generation”, *Opt. Express*, Vol. 20, no. 2, pp. 1685-1690, Jan. 2012.
- [42] K. J. Blow and D. Wood, “Theoretical description of transient stimulated Raman scattering in optical fibers,” *IEEE J. Quantum Electron.*, vol. 25, no. 12, pp. 2665-2673, Dec. 1989.
- [43] J. Cardenas, C. B. Poitras, K. Luke, L.-W. Luo, P. A. Morton, and M. Lipson, “High coupling efficiency etched facet tapers in silicon waveguides,” *IEEE Photon. Technol. Lett.*, vol. 26, no. 23, pp. 2380-2382, Dec. 2014.
- [44] S. Wang, J. Hu, H. Guo, and X. Zeng, “Optical Cherenkov radiation in an  $As_2S_3$  slot waveguide with four zero-dispersion wavelengths,” *Opt. Express.*, vol. 21, no. 3, pp. 3067-3072, Jan. 2013.
- [45] I. W. Hsieh, X. Chen, X. Liu, J. I. Dadap, N. C. Panoiu, C. Y. Chou, F. Xia, W. M. Green, Y. A. Vlasov, and R. M. Osgood, “Supercontinuum generation in silicon photonic wires,” *Opt. Express.*, vol. 15, no. 23, pp. 15242-15249, Nov. 2007.
- [46] S. J. Madden, D-Y. Choi, D. A. Bulla, A. V. Rode, B. Luther-Davies, V.G. Ta’eed, M.D. Pelusi and B.J. Eggleton, “Long, low loss etched  $As_2S_3$  chalcogenide waveguides for all-optical signal regeneration,” *Opt. Express*, Vol. 15, no. 22, pp. 14414-14421, Oct. 2007.
- [47] J. J. Hu, N. N. Feng, N. Carlie, L. Petit, A. Agarwal, K. Richardson and L. Kimerling, “Optical loss reduction in high-index-contrast chalcogenide glass waveguides via thermal reflow,” *Opt. Express*, Vol. 18, no. 2, pp. 1469-1478, Jan. 2010.
- [48] G. P. Agrawal, “Chapter 6 optical pulse compression,” in *Applications of nonlinear fiber optics*, 2ed. San Francisco, CA, USA: Academic, 2009, pp. 561-587.
- [49] P. K. A. Wai, H. H. Chen, and Y. C. Lee, “Radiations by “solitons” at the zero group-dispersion wavelength of single-mode optical fibers,” *Phys. Rev. A*, vol. 41, no. 1, pp. 426-439, Jan. 1990.
- [50] J. M. Dudley and S. Coen, “Supercontinuum generation in photonic crystal fiber,” *Rev. Mod. Phys.*, vol. 78, pp. 1135-1184, Dec. 2006.
- [51] K. Senthilnathan, Q. Li, K. Nakkeeran, and P. K. A. Wai, “Robust pedestal-free pulse compression in cubic-quintic nonlinear media,” *Phys. Rev. A* 78, pp.1-12, 2008.
- [52] Q. Li, K. Senthilnathan, K. Nakkeeran, and P. K. A. Wai, “Nearly chirp-and pedestal-free pulse compression in nonlinear fiber Bragg gratings,” *J. Opt. Soc. Am. B.*, vol. 26, no. 3, pp. 432-443, Mar. 2009.